Journal of the Mechanics and Physics of Solids 78 (2015) 511–525

Contents lists available at ScienceDirect

Journal of the Mechanics and Physics of Solids

journal homepage: www.elsevier.com/locate/jmps

Modeling hydrogen transport by dislocations

Mohsen Dadfarnia [a,e], May L. Martin [b,e], Akihide Nagao [c,e], Petros Sofronis [a,b,e,*], Ian M. Robertson [d,e]

[a] Department of Mechanical Science and Engineering, University of Illinois at Urbana-Champaign, 1206 West Green Street, Urbana, IL 61801, USA
[b] Department of Materials Science and Engineering, University of Illinois at Urbana-Champaign, 1304 West Green Street, Urbana, IL 61801, USA
[c] Material Surface and Interface Science Research Department, Steel Research Laboratory, JFE Steel Corporation, Minamiwatarida-cho, Kawasaki-ku, Kawasaki, Kanagawa 210-0855, Japan
[d] Department of Materials Science and Engineering, University of Wisconsin-Madison, 1415 Engineering Drive, Madison, WI 53706, USA
[e] International Institute for Carbon-Neutral Energy Research (WPI-I2CNER), Kyushu University, 744 Motooka, Nishi-ku, Fukuoka, Fukuoka 819-0395, Japan

ARTICLE INFO

Article history:
Received 15 September 2014
Received in revised form
6 January 2015
Accepted 8 March 2015
Available online 10 March 2015

Keywords:
Hydrogen embrittlement
Hydrogen transport
Dislocation

ABSTRACT

Recent experimental studies of the microstructure beneath fracture surfaces of specimens fractured in the presence of high concentrations of hydrogen suggest that the dislocation structure and hydrogen transported by mobile dislocations play important roles in establishing the local conditions that promote failure. The experiments demonstrate that hydrogen is responsible for the copious plasticity in large volumes of material before the onset of fracture and further afield from a crack tip. A revised model for hydrogen transport that accounts for hydrogen carried by dislocations along with stress driven diffusion and trapping at other microstructural defects is proposed. With the use of this new model, numerical simulation results for transient hydrogen profiles in the neighborhood of a crack tip are presented. Based on hydrogen-enhanced dislocation mobility and density, the results indicate that dislocation transport can contribute to the elevation of the local hydrogen concentrations ahead of the crack to levels above those predicted by the classical diffusion model and to distributions that extend farther afield.

1. Introduction

Recent experimental observations of the evolved microstructure in metals containing high concentrations (a few thousands at. ppm) of solute hydrogen suggest that hydrogen not only accelerates the evolution of the microstructure but also stabilizes it in unanticipated configurations (Martin et al., 2011a, 2011b, 2012a, 2013, 2012b, 2014; Nagao et al., 2012; Wang et al., 2014). In every case the evolved microstructure was found to be more complex than would be envisioned based on prior assumed knowledge of dislocation behavior in the presence or absence of hydrogen. Key features in these studies are that the evolved microstructure is indicative of very high strains and in some situations exists in configurations that do not conform to the accepted evolution pathway. The enhanced evolution was explained in terms of the hydrogen-enhanced

* Corresponding author at: Department of Mechanical Science and Engineering, University of Illinois at Urbana-Champaign, 1206 West Green Street, Urbana, IL 61801, USA. Fax: +1 217 244 6534.
E-mail address: sofronis@illinois.edu (P. Sofronis).

http://dx.doi.org/10.1016/j.jmps.2015.03.002
0022-5096/

dislocation activity, which is motivated by the hydrogen-enhanced localized plasticity (HELP) mechanism (Sofronis and Birnbaum, 1995; Robertson, 2001). In addition, since hydrogen must travel with the dislocations, a requisite for the continued operation of the HELP mechanism, the hydrogen concentration must be increased in the regions of the evolved microstructure.

Hydrogen transport by mobile dislocations is not a new concept; it was first suggested by Bastien and Azou (1951) and is supported by numerous experimental observations (Kurkela and Latanision, 1979; Hwang and Bernstein, 1986; Windle and Smith, 1968; Itoh et al., 1997; Nagao et al., 1998; Frankel and Latanision, 1986). Models for hydrogen transport by dislocations have been proposed by Tien et al. (1975, 1976) and Tien (1976). These dislocation transport models yield much faster diffusion rates than lattice diffusion and support the idea that dislocations can carry hydrogen deep into a specimen gage section or plastic zone even at ambient temperatures. Associated with these models by Tien is the proposition that local hydrogen supersaturations develop through stripping of the solutes off the moving dislocations by traps. On the other hand, theoretical analysis by Hirth and Johnson (1983) points out that transport of hydrogen by dislocations in iron or steel at room temperature produces only small supersaturations at internal trap sites; larger supersaturations by dislocation transport are predicted to be possible in metals with much smaller diffusivities for hydrogen, e.g. nickel. A secondary but important consequence of the attendant hydrogen concentration associated with the dislocations is that it reduces the interaction energy between dislocations allowing them to pack more densely. It will also stabilize the microstructure preventing reorganization since an additional driving force would have to be provided to first remove hydrogen from the dislocations to permit reorganization (Ferreira et al., 1998).

This hydrogen-induced acceleration of the evolved microstructure is not confined to the volume of the crack tip plastic zone but extends, as it must, throughout the deforming volume. In addition, it must occur from the onset of plastic deformation. A consequence of this is that the microstructure into which a crack must propagate is evolved and characterized as being highly strained with a high hydrogen content. Indeed the local hydrogen content is likely to be higher than the enhancement achievable in the hydrostatic stress peak location ahead of a crack tip as predicted by the classic diffusion model. The mechanism for such widespread hydrogen accumulation is transport by mobile dislocations whose mobility is further accentuated by the HELP mechanism – a distribution and accumulation mechanism that has yet to be considered fully.

For example, in considering hydrogen-induced intergranular failure, it is known that a critical level of hydrogen must be established on the grain boundaries before the failure mode will transition from transgranular to intergranular (Lassila and Birnbaum, 1986, 1987, 1988). It was assumed that this critical concentration was achieved by diffusion, which may be enhanced by diffusion along grain boundaries. For example, Ladna and Birnbaum (1987) determined the diffusion of deuterium along grain boundaries in nickel and found it to be enhanced along high energy 39° ⟨110⟩ symmetrical tilt boundaries ($\Sigma=9$) but not along low energy 129° ⟨110⟩ symmetric tilt boundaries ($\Sigma=11$). However, based on experimental observations of the evolved microstructure immediately beneath hydrogen-induced intergranular facets in Ni (Martin et al., 2012a), a martensitic alloy (Nagao et al., 2012) and Fe (Wang et al., 2014), Sofronis, Robertson and coworkers suggested that the interaction of hydrogen-carrying dislocations with grain boundaries played an important role in establishing the conditions for promoting transition of the failure mode from transgranular to intergranular. They proposed that as transfer of strain across an interface does not necessarily involve equal numbers of dislocations absorbed and ejected by the interface (Lee et al., 1990a, 1990b; Clark et al., 1992), there will be an increase in the accumulated hydrogen at some interfaces. In addition, the process of slip transfer causes a change in the grain boundary energy as there will be a net difference in the Burgers vectors of the absorbed and ejected dislocations that remains in the grain boundary (Lee et al., 1990b; Clark et al., 1992). This effect will be magnified in the presence of hydrogen because of the attendant enhancement of the dislocation velocity. The increased strain energy density due to the residual grain boundary dislocations created by the act of slip transfer and the increase in hydrogen concentration on the grain boundary along with the elevated stress due to the evolved microstructure around the grain boundaries all contribute to promote intergranular failure. Of course, this mechanism is not restricted to hydrogen-induced intergranular failure, it must operate even if the failure mode remains ductile. Indeed, the evolved microstructure has been seen to be enhanced in other failure modes (Martin et al., 2011a, 2011b, 2013). Sofronis, Robertson and coworkers suggested that hydrogen-induced failure be more appropriately termed hydrogen-accelerated plasticity mediated failure. The specific final failure may be by a particular mechanism but the conditions for determining the failure mode and path is determined by the preceding plasticity, the local stress state, and hydrogen concentration established by these two factors.

The experimental evidence for dislocation assisted transport combined with the evidence of extensive plasticity prior to hydrogen-assisted failure suggests dislocation transport of hydrogen may be a critical component of the failure mechanism. For, in addition to the extent of the plasticity, the degree of plasticity is observed to be remarkably more advanced than predicted or observed in the absence of hydrogen. In other words, there is sufficient hydrogen to affect dislocation behavior further from the crack tip than expected by current transport models. The transport by dislocations seems best suited as a candidate to account for this disparity in hydrogen concentration.

To date, in simulations of hydrogen transport in elastoplastically deforming materials, hydrogen trapping and stress-driven hydrogen diffusion were accounted for, but, the effect of transport of hydrogen by moving dislocations was neglected as was the accelerated generation, recombination and annihilation of dislocations due to the presence of hydrogen (Sofronis and McMeeking, 1989; Taha and Sofronis, 2001; Dadfarnia et al., 2009; Novak et al., 2010). In this work, the model by Taha and Sofronis (2001) and Dadfarnia et al. (2009) to determine hydrogen profiles ahead of a crack tip is extended to take into

account hydrogen transport by dislocations as well as to introduce a simple multiplication factor to allow incorporation of dislocation generation/trapping and dislocation velocity enhancements due to hydrogen. This is the first step toward capturing in a model the complex microstructural state observed experimentally in the presence of hydrogen. Thus, although the present model does not address the fracture mechanism(s) per se, it does address an aspect of the transport issue which is important to the understanding the conditions governing fracture.

The paper is organized as follows: First, the mathematical modeling issues of the coupled hydrogen diffusion and elastoplastic problem is outlined in Section 2. Next, the numerical simulation results for transport of hydrogen under small scale yielding conditions are presented for a body-centered cubic (bcc) steel (low solubility and high diffusivity system) and face-centered cubic (fcc) steel (high solubility and low diffusivity system) in Section 3. The interaction of hydrogen transport with material parameters and hydrogen uptake conditions are explored in Section 4 and conclusions are drawn in Section 5.

2. Hydrogen transport in an elastoplastically deforming solid

As in previous models (Sofronis and McMeeking, 1989; Taha and Sofronis, 2001), it is assumed that hydrogen atoms reside either at normal interstitial lattice sites (NILS) or are trapped reversibly at mobile and immobile dislocations. For the sake of analysis, we ignore trapping at other microstructural defects – analysis of how such additional trapping affects hydrogen transport can be found in Dadfarnia et al. (2011). An additional assumption is that the transport of hydrogen takes place through NILS diffusion and by mobile dislocations.

NILS and trapped hydrogen populations at dislocations are in equilibrium according to Oriani's theory (Oriani, 1970) such that

$$\frac{\theta_T}{1-\theta_T} = \frac{\theta_L}{1-\theta_L}\exp\left(\frac{W_B}{RT}\right), \tag{1}$$

where θ_L is the NILS occupancy, θ_T is the trapping site occupancy, W_B is the trap binding energy, $R=8.314$ J/mol K is the universal gas constant, and T is the absolute temperature. The NILS hydrogen concentration, C_L, measured in hydrogen atoms per unit volume, can be expressed as:

$$C_L = \theta_L \beta N_L, \tag{2}$$

where β denotes the number of NILS per solvent atom, N_L denotes the number of solvent atoms per unit volume given by $N_L = N_A/V_M$ with $N_A = 6.0232\times 10^{23}$ atoms/mol being Avogadro's number, and V_M the molar volume of the host lattice measured in units of volume per mole. Similarly, the hydrogen concentration at dislocation traps (mobile and immobile), C_T, measured in hydrogen atoms per unit volume, can be written as

$$C_T = \theta_T \alpha N_T, \tag{3}$$

where α denotes the number of trapping sites per dislocation trap and N_T denotes the dislocation trap density (mobile and immobile) in number of traps per unit volume. Through Eqs. (1)–(3), one can express the hydrogen concentration at trapping sites in terms of the lattice concentration.

The dislocation trap density can be determined experimentally as a function of the plastic strain, $N_T(\varepsilon^p)$, with ε^p being the effective plastic strain (Kumnick and Johnson, 1980). If experimental data are not available, assuming one trap per atomic plane threaded by a dislocation line (Tien et al., 1976; McLellan, 1979), the dislocation trap density can be written in terms of the total dislocation density ρ (mobile and immobile), which is a function of the plastic strain, as

$$N_T = \lambda(\rho/a), \tag{4}$$

where a is the lattice parameter and $\lambda = \sqrt{2}$ or $\sqrt{3}$ for bcc and fcc lattices, respectively. Here hydrogen will affect the dislocation trap density as it enhances the generation of mobile dislocations as well as the density of immobile dislocations through accelerated interactions. By virtue of Eq. (4), the density of traps (number per unit volume) associated with mobile dislocations becomes:

$$N_T^m = \lambda(\rho_m/a), \tag{5}$$

where ρ_m is the mobile dislocation density.

Extension of the model of Sofronis and McMeeking (1989) to account for dislocation transport yields the governing equation of hydrogen transport as:

$$\frac{\partial}{\partial t}(C_L + C_T) + \nabla\cdot(\mathbf{J} + \mathbf{J^d}) = 0, \tag{6}$$

where

$$\mathbf{J} = -D\nabla C_L + \frac{DV_H}{3RT} C_L \nabla\sigma_{kk} \tag{7}$$

is the hydrogen flux through NILS motivated by chemical potential gradients and

$$\mathbf{J^d} = (N_T^m\,\mathbf{V^d})(\alpha\theta_T) \tag{8}$$

is the hydrogen flux associated with mobile dislocations. Moving dislocations represent moving traps that carry hydrogen atoms. The flux of these moving traps is $N_T^m\,\mathbf{V^d}$, where $\mathbf{V^d}$ is the dislocation velocity vector. Hence the corresponding hydrogen flux $\mathbf{J^d}$ results by considering the number $\alpha\theta_T$ of occupied sites per moving trap. In Eqs. (6) and (7), D is the hydrogen diffusion coefficient through NILS, V_H is the partial molar volume of hydrogen in solid solution, σ_{kk} is the trace of the stress tensor, $\partial/\partial t$ denotes partial derivative with respect to time, ∇ is the gradient operator, and $(\cdot)$ denotes divergence.

Substitution of Eqs. (7) and (8) into (6) with

$$\frac{\partial C_T}{\partial t} = \frac{\partial C_T}{\partial C_L}\frac{\partial C_L}{\partial t} + \frac{\partial C_T}{\partial N_T}\frac{dN_T}{d\varepsilon^p}\frac{d\varepsilon^p}{dt}, \tag{9}$$

where d/dt denotes time differentiation, provides the governing equation for transient hydrogen transport accounting for hydrostatic drift and dislocation transport:

$$\frac{D}{D_{eff}}\frac{\partial C_L}{\partial t} + \alpha\theta_T\frac{dN_T}{d\varepsilon^p}\frac{d\varepsilon^p}{dt} - D\nabla^2 C_L + \nabla\cdot\left(\frac{DV_H}{3RT}C_L\nabla\sigma_{kk}\right) + \nabla\cdot\left(\alpha\theta_T N_T^m\,\mathbf{V^d}\right) = 0, \tag{10}$$

where D_{eff} is an effective diffusion coefficient given by

$$\frac{D}{D_{eff}} = 1 + \frac{\partial C_T}{\partial C_L} = 1 + \frac{K_T\alpha\beta N_L N_T}{[\beta N_L + (K_T - 1)C_L]^2}. \tag{11}$$

where $K_T = \exp(W_B/RT)$. By introducing the following non-dimensional parameters

$$\xi_i = \frac{x_i}{L}, \quad \tau = \frac{Dt}{L^2}, \quad \phi = \frac{C_L}{C_0}, \quad \psi = \frac{\sigma_{kk}V_H}{3RT}, \tag{12}$$

where x_i is location coordinate, L is a non-dimensionalizing length, and C_0 is a reference hydrogen concentration, Eq. (10) is recast as follows:

$$\frac{D}{D_{eff}}\frac{\partial\phi}{\partial\tau} + \frac{\alpha\theta_T}{C_0}\frac{dN_T}{d\varepsilon^p}\frac{d\varepsilon^p}{d\tau} - \frac{\partial^2\phi}{\partial\xi_i\partial\xi_i} + \frac{\partial}{\partial\xi_i}\left(\phi\frac{\partial\psi}{\partial\xi_i}\right) + \frac{\partial}{\partial\xi_i}\left(\frac{\alpha\theta_T N_T^m}{C_0}\frac{V_i^d}{D/L}\right) = 0. \tag{13}$$

The transport model as described by Eqs. (10) or (13) considers that hydrogen is transported by mobile dislocations in addition to its diffusion through NILS. Hydrogen that is trapped in mobile and immobile dislocations as described by Eq. (3) is not participating in the diffusion process through NILS. The last term of Eq. (13) indicates that the contribution of the hydrogen transport by dislocations to the development of the hydrogen concentrations in NILS is stronger in systems with lower lattice diffusion, D.

3. Application of the dislocation transport model

For the numerical solution of the hydrogen transport Eqs. (10) or (13), the material is assumed to deform plastically with an associated flow rule based on von Mises yielding. The mobile dislocation density is calculated through the classical Orowan equation

$$\dot{\varepsilon}^p = \rho_m b v^d, \tag{14}$$

where v^d is the magnitude of the dislocation velocity, $v^d = \|\mathbf{V}^d\|$, and b is the magnitude of the Burgers vector of the dislocations. For a given plastic strain rate, Eqs. (5) and (14) furnish $N_T^m v^d = \lambda\dot{\varepsilon}^p/ba$ for the magnitude of the vector $N_T^m\,\mathbf{V^d}$ that appears in the last term of Eq. (10) to describe hydrogen transport by dislocations. For simplicity, a specific direction of the dislocation velocity vector is input to the solution process and is assumed constant throughout the deforming body. Note that in this model the spatial variation of the direction of the dislocation motion, which relates to the evolution of the microstructure, is not taken into account. Once this evolution can be quantified, the present model can easily be modified to address dislocation motion directions that vary spatially.

In order to account for the effect of hydrogen on increasing the density of dislocation traps (mobile and immobile) and the velocity of mobile dislocations during plastic straining, we solve the transport Eq. (10) by considering that the density of dislocation traps is $n_T N_T$ instead of N_T and the mobile dislocation velocity is $n_d v^d$ instead of v^d, where n_T and n_d are multiplying factors. The same multiplying factor n_T is used for the density of traps associated with the mobile dislocations, N_T^m. Thus, the effect of hydrogen on the dislocation density and velocity will be studied through a parametric study over the parameters n_T and n_d, which is a simplifying assumption for the treatment of the hydrogen effect. Here, for purposes of demonstrating the impact of hydrogen transport by dislocations, the effect of the hydrogen-induced dislocation density and

velocity increases on the material constitutive behavior, and, hence, on the full coupling of the transport equation to the elastoplastic deformation of the material are not included. Full coupling could be done by considering the effect of the increased dislocation density on the work hardening rate of the material, and this is a subject of a future effort. Alternatively, full coupling between hydrogen transport and elastoplastic deformation could be included through a dislocation-based constitutive model for the deforming solid with appropriate evolution laws for the mobile and immobile dislocation densities in the presence of hydrogen. To fully capture the evolved microstructure, the introduction of dislocation-based constitutive models would need to be coupled with self-organization of the dislocations into a cell structure and its impact on hydrogen trapping sites and dislocation mobilities.

The initial/boundary-value problem for hydrogen transport and elastoplastic deformation is solved near a blunting crack tip in plane strain and in the presence of gaseous hydrogen inside the crack at 1 atm (0.1 MPa) pressure. The coupling between the two problems is through the effect of stress on lattice diffusion and plastic straining on the density of traps (Sofronis and McMeeking, 1989; Liang and Sofronis, 2003). The boundary layer approach of small scale yielding (SSY) under mode I opening with the asymptotic displacements of the Irwin singular linear elastic field (Irwin, 1960) imposed on the outer boundary of the domain of analysis located at a distance L from the crack tip is considered. For the crack faces, traction free boundary conditions are considered as the stress intensity factor due to the applied hydrogen gas pressure on the crack surfaces is negligible. The hydrogen-related boundary and initial conditions are shown in Fig. 1: zero concentration boundary condition ($C_L = 0$) on the outer domain boundary, zero flux boundary condition ($\mathbf{J}\cdot\mathbf{n} = 0$) along the axis of symmetry ahead of the crack tip, and a constant NILS hydrogen concentration ($C_L = C_0$) on the crack surfaces in equilibrium with the hydrogen gas. The material is hydrogen-free at time zero. Displacements on the remote boundary are applied at L=30 mm incrementally at a constant stress intensity factor rate $\dot{K}_I$ toward a final value K_I. As the applied displacements increase, hydrogen diffuses into the material through the crack faces. Although the T-stress affects the hydrogen interaction with the material deformation (Liang et al., 2004), this effect is neglected in this study. An initially blunted crack tip with an opening displacement $\delta_{t0} = 10\ \mu\text{m}$ is considered.

The hydrogen-related boundary and initial conditions are relevant to hydrogen containment pressurized vessels and environmental hydrogen embrittlement whereby the crack faces are exposed to a pressurized hydrogen atmosphere. We assumed in this work that hydrogen dissociation is fast and equilibrium is rapidly attained on the crack surface (Staykov et al., 2014). Therefore, the boundary conditions on the crack faces are associated with a constant hydrogen concentration which is the result of the equilibration of the surface hydrogen with the gaseous hydrogen under a given pressure. The effect of boundary conditions on the hydrogen uptake when such equilibrium is not the case, e.g. in the presence of surface impurities, is the subject of a subsequent publication.

Two model systems were considered with one representing a high diffusivity and low solubility bcc metal and the other a low diffusivity and high solubility fcc metal. The material parameters given in Table 1 are of a bcc X70/X80 pipeline and a forged Nitronic 40 (21Cr–6Ni–9Mn) austenitic fcc stainless steel although the resultant calculations should be considered representative of the system rather than a specific material. The calculations were performed for the dislocation velocity vector pointing away from the crack tip and either parallel to the crack faces (1-direction in Fig. 1) or along a direction at a 45° angle to them.

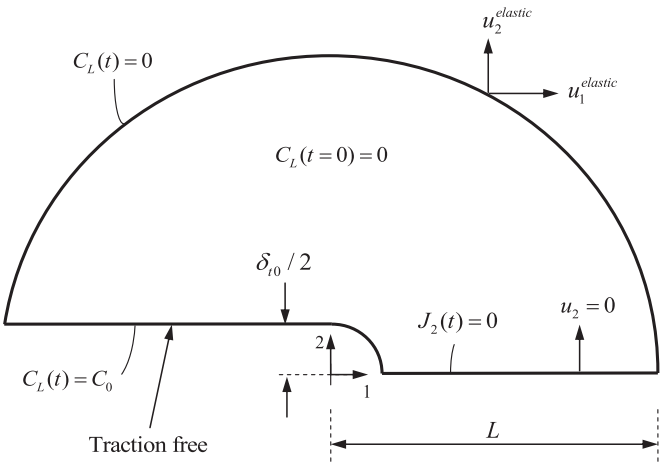

Fig. 1. Description of initial and boundary conditions for the coupled elastoplastic and hydrogen transport problems at a blunting crack tip. The parameter δ_{t0} denotes the initial crack tip opening, and $u_1^{elastic}$ and $u_2^{elastic}$ are the asymptotic displacements fields in 1- and 2-directions, respectively. The parameter C_0 is normal interstitial lattice site (NILS) hydrogen concentration at the crack faces in equilibrium with the hydrogen gas inside the crack. Symmetry dictates that displacement u_2 and hydrogen flux J_2 is zero along the axis of symmetry ahead of the crack tip.

Table 1
Material properties of bcc X70/X80 pipeline steel and forged Nitronic 40 austenitic fcc stainless steel.

Properties	*Symbol*	*Value*	
		X70/X80	*Forged Nitronic 40*
Young's modulus (GPa)	E	200	200
Poisson's ratio	ν	0.3	0.3
Yield stress (MPa)	σ_0	600	660
Work hardening exponent	n	0.06	0.1
Number of sites per dislocation trap	α	10 (Liang et al., 2008; Hirth and Carnahan, 1978)	10 (Liang et al., 2008; Hirth and Carnahan, 1978)
Number of NILS per host atom	β	1	1
Dislocation trap binding energy (kJ/mol)	W_B	50	10 (Thomas, 1981)
Trap density (Mobile and immobile dislocations)	N_T	Kumnick and Johnson (1980)	Eq. (4)
Molar volume of the host lattice (m^3/mol)	V_M	7.11×10^{-6}	7.11×10^{-6}
Partial molar volume of H (m^3/mol)	V_H	2×10^{-6} (Hirth, 1980; Moody et al., 1990)	2×10^{-6} (Moody et al., 1990)
Diffusion coefficient (m^2/s)	D	2×10^{-8} (Hirth, 1980)	2×10^{-16} (San Marchi et al., 2007)
Solubility at 300 K ($molH_2/m^3\sqrt{MPa}$)	K	0.005434 (Hirth, 1980)	20.85 (San Marchi et al., 2007)
Lattice parameter (nm)	a	0.287	0.358
Magnitude of the Burgers vector (nm)	b	0.248	0.253

3.1. BCC case

The simulation domain was loaded at a stress intensity factor rate $\dot{K}_I = 0.05\ \mathrm{MPa}\sqrt{\mathrm{m}}/\mathrm{s}$ from the stress-free condition to $K_I = 100\ \mathrm{MPa}\sqrt{\mathrm{m}}$. During loading, a constant NILS hydrogen concentration $C_L = C_0 = 2.084\times10^{21}$ H atoms/m^3 ($=2.46\times10^{-8}$ H atoms per solvent atom) was prescribed on the crack faces in equilibrium with hydrogen gas at a pressure of 1 atm. A hydrogen binding energy $W_B = 50$ kJ/mol was selected to reflect trapping with dislocation debris. The effect of changing the binding energy is explored in Section 4.2. The trap density N_T was assumed to increase with plastic straining as in Kumnick and Johnson (1980).

Fig. 2 shows the effect of dislocation transport on the development of the normalized hydrogen concentration in NILS and trapping sites (C_L/C_0 and C_T/C_0, respectively) ahead of the crack tip at the end of loading, $K_I = 100\ \mathrm{MPa}\sqrt{\mathrm{m}}$, and with the dislocation direction parallel to the crack faces. The distance ahead of the crack tip R is normalized by the crack tip opening displacement $\delta_t = 48.16\ \mu\mathrm{m}$ at $K_I = 100\ \mathrm{MPa}\sqrt{\mathrm{m}}$. The results for $n_d = 0$ represent transport only through NILS. Fig. 2a shows the hydrogen profiles under the assumption that hydrogen does not influence the dislocation density, $n_T = 1$, but it does influence the dislocation velocity. The peak NILS hydrogen concentration, when hydrogen transport by dislocations is accounted for with a tenfold increase of the dislocation velocity ($n_d = 10$), is about 40% higher than that for transport through NILS only ($n_d = 0$). The hydrogen concentrations at trapping sites are almost the same for all values of n_d because the dislocation traps are practically saturated due to the high binding energy, $W_B = 50$ kJ/mol. As expected, the trapped populations attain their maxima at the crack tip where the plastic straining is higher and NILS concentration peak coincides with the location of the hydrostatic stress peak. Lastly, the trapping concentrations near to the crack tip are orders of magnitude greater than the lattice concentrations. Although the trapping site density, αN_T, is smaller than the NILS density, βN_L, the

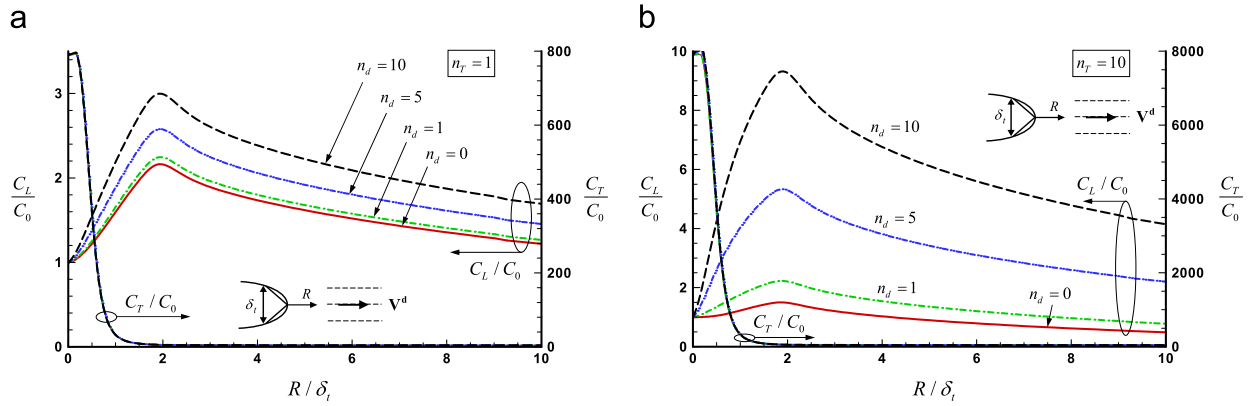

Fig. 2. Plot of normalized hydrogen concentration in NILS, C_L/C_0, and trapping sites, C_T/C_0, vs. normalized distance R/δ_t from the crack tip along the axis of symmetry for the *bcc* steel at $K_I = 100\ \mathrm{MPa}\sqrt{\mathrm{m}}$: (a) $n_T = 1$ and (b) $n_T = 10$. The dislocation effect on transport is explored through the parameters n_T and n_d which denote the effect of hydrogen respectively on dislocation density and velocity during plastic straining. The direction of the dislocation velocity vector $\mathbf{V^d}$ with respect to the crack plane is shown on the figure. The crack opening displacement is $\delta_t = 48.16\ \mu\mathrm{m}$ and $C_0 = 2.084\times10^{21}$ H atoms/m^3 (2.46×10^{-8} H atoms per solvent atom) is NILS hydrogen concentration at the crack surface in equilibrium with hydrogen gas pressure of 1 atm.

occupancy of the trapping sites, θ_T, is much larger than the NILS occupancy, θ_L, which leads to high ratios of trapping to lattice site concentrations according to $C_T/C_L = (\alpha N_T/\beta N_L)(\theta_T/\theta_L)$. The impact of hydrogen increasing the dislocation density on the hydrogen profiles is shown in Fig. 2b; n_T was increased from 1 to 10. The difference between the trap concentration magnitudes in Fig. 2a and b is due to the corresponding difference in the trap density, namely $n_T = 1$ vs. $n_T = 10$. By comparing the two sets of profiles shown in Fig. 2, it is evident that dislocation transport has a profound effect on the magnitude of the NILS concentration when hydrogen increases both the dislocation density and velocity during plastic deformation. In fact for a tenfold increase of both dislocation density and velocity, the NILS concentration at the peak location is calculated to be about 520% higher than in the absence of dislocation transport. For this enhancement to be maintained, active loading is required. In other words, if the load remains constant at its peak value $K_I = 100\ \mathrm{MPa}\sqrt{\mathrm{m}}$ the normalized peak value of NILS hydrogen concentration would settle to $C_L/C_0 \approx 2.7$ at $R/\delta_t = 2$ at the steady state (Dadfarnia et al., 2009).

The impact on the normalized hydrogen concentration in NILS, C_L/C_0, of changing the direction of the dislocation velocity vector $\mathbf{V^d}$ to an angle of 45° to the crack plane is shown in Fig. 3. The peak hydrogen concentration ahead of the crack tip is slightly smaller than when the dislocation velocity direction is along the axis of symmetry (Fig. 2). Obviously, in this case, dislocations transport hydrogen away from the symmetry line. Lastly, Fig. 3b shows that on increasing the dislocation density and velocity ($n_T = 10$, $n_d = 10$), the rate of hydrogen transported by dislocations becomes faster than that by hydrogen delivered through lattice diffusion. A consequence of this is that lattice concentrations very close to the crack tip are lower than those in the absence of dislocation transport. The effect of changing the direction of the dislocation velocity on the hydrogen accumulation near the crack tip can be clearly seen from the contour plots of the normalized NILS hydrogen concentration shown in Fig. 4. These effects certainly need to be taken into consideration in dislocation models for fracture that are based on dislocation pileups emanating from the crack tip (Gerberich et al., 1996).

These two cases illustrate that hydrogen will be transported from the crack tip region into the lattice. If prior deformation had generated a dislocation cell structure, this dislocation transport of hydrogen from the crack tip would provide a means of rapidly delivering hydrogen to it. This would modify the dislocation structure in the cell wall by allowing dislocations, through the hydrogen shielding mechanism, to reside closer together. It also would influence subsequent dislocation emission and accommodation processes within the cell walls.

3.2. FCC case

Similar to the bcc case, the fcc material domain was loaded from the stress-free state to $K_I = 100\ \mathrm{MPa}\sqrt{\mathrm{m}}$. However, due to the slow diffusivity of hydrogen in fcc steels, a lower stress intensity factor rate $\dot{K}_I = 0.01\ \mathrm{MPa}\sqrt{\mathrm{m}}/s$ was considered. The crack tip opening displacement at the end of loading was $\delta_t = 40.99\ \mu\mathrm{m}$. During loading, a constant NILS hydrogen concentration $C_L = C_0 = 7.996 \times 10^{24}$ H atoms/m^3 ($=9.44 \times 10^{-5}$ H atoms per solvent atom) was prescribed on the crack faces in equilibrium with hydrogen gas at 1 atm. The trap density was calculated through Eq. (4) in which $\lambda = \sqrt{3}$. The total dislocation density was assumed to increase linearly with plastic strain (Gilman, 1969), that is, $\rho = \rho_0 + \gamma\varepsilon^p$ for $\varepsilon^p \le 0.5$ and $\rho = \text{const.}$ for $\varepsilon^p > 0.5$, where $\gamma = 2 \times 10^{16}$ line length/m^3 and $\rho_0 = 10^{10}$ line length/m^3 was assumed to be the density in the unstrained material.

Fig. 5 shows the normalized NILS and trapped hydrogen concentration profiles ahead of the crack tip at the end of loading, $K_I = 100\ \mathrm{MPa}\sqrt{\mathrm{m}}$, when the direction of dislocation velocity is along the crack plane. Clearly, dislocations carry the hydrogen entering through the crack faces to locations further from the crack than achievable by diffusion alone. In contrast,

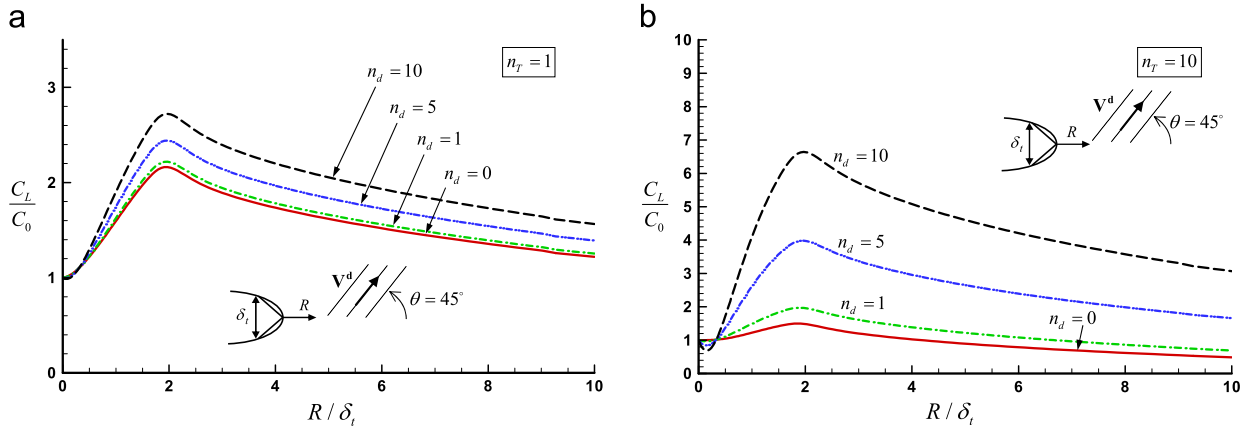

Fig. 3. Normalized NILS hydrogen concentration C_L/C_0 ahead of the crack tip for the *bcc* steel at $K_I = 100\ \mathrm{MPa}\sqrt{\mathrm{m}}$ accounting for the effect of dislocation transport of hydrogen with the direction of the dislocation velocity vector $\mathbf{V^d}$ with respect to the crack plane shown in the figure: (a) $n_T = 1$ and (b) $n_T = 10$. The dislocation effect on transport is explored through the parameters n_T and n_d which denote the effect of hydrogen respectively on dislocation density and velocity during plastic straining. The crack opening displacement is $\delta_t = 48.16\ \mu\mathrm{m}$ and $C_0 = 2.084 \times 10^{21}$ H atoms/m^3 (2.46×10^{-8} H atoms per solvent atom).

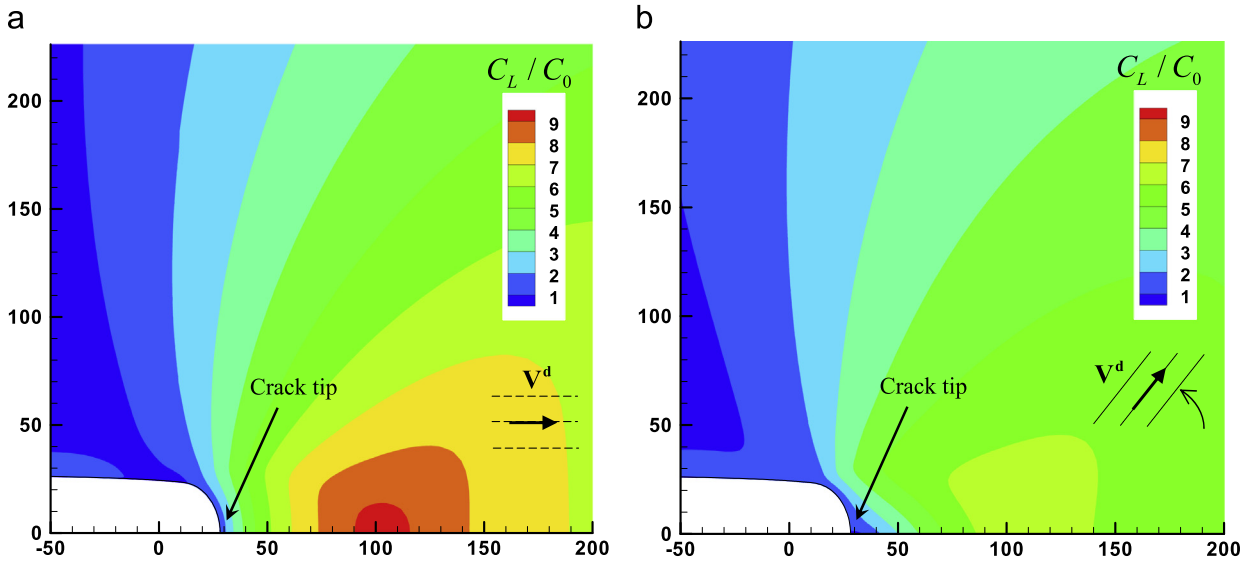

Fig. 4. Contour plots of normalized NILS hydrogen concentration C_L/C_0 near the crack tip for the *bcc* steel at $K_I = 100\ \text{MPa}\sqrt{\text{m}}$ when the dislocation velocity $\mathbf{V^d}$ is (a) parallel to crack plane and (b) at an angle of 45° with the crack plane. $C_0 = 2.084 \times 10^{21}$ H atoms/m^3 (2.46×10^{-8} H atoms per solvent atom), $n_T = 10$ and $n_d = 10$. Dimensions are in microns.

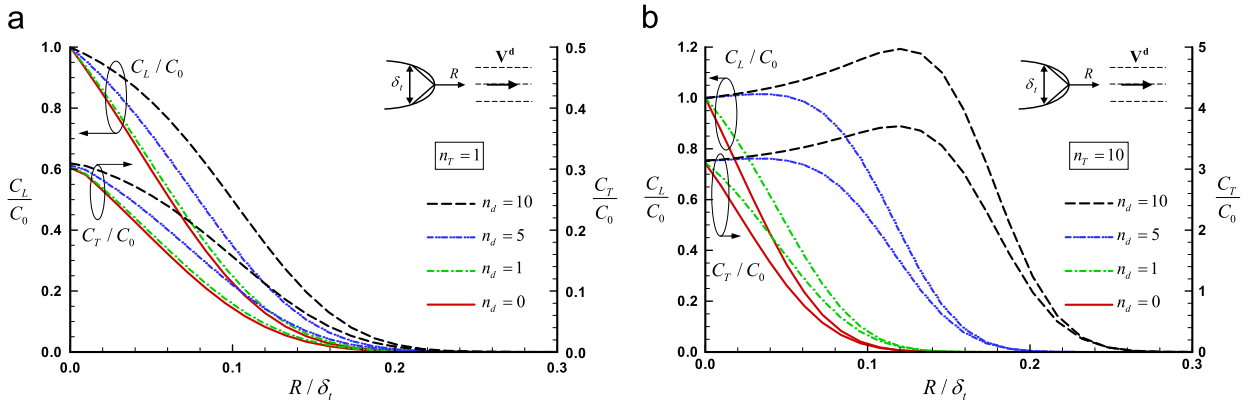

Fig. 5. Plot of normalized hydrogen concentration in NILS C_L/C_0 and trapping sites C_T/C_0 vs. normalized distance R/δ_t from the crack tip along the axis of symmetry for the *fcc* steel at $K_I = 100\ \text{MPa}\sqrt{\text{m}}$: (a) $n_T = 1$ and (b) $n_T = 10$. The crack opening displacement is $\delta_t = 40.99\ \mu\text{m}$ and $C_0 = 7.996 \times 10^{24}$ H atoms/m^3 (9.44×10^{-5} H atoms per solvent atom). The direction of the dislocation velocity vector $\mathbf{V^d}$ with respect to the crack plane is shown on the figure.

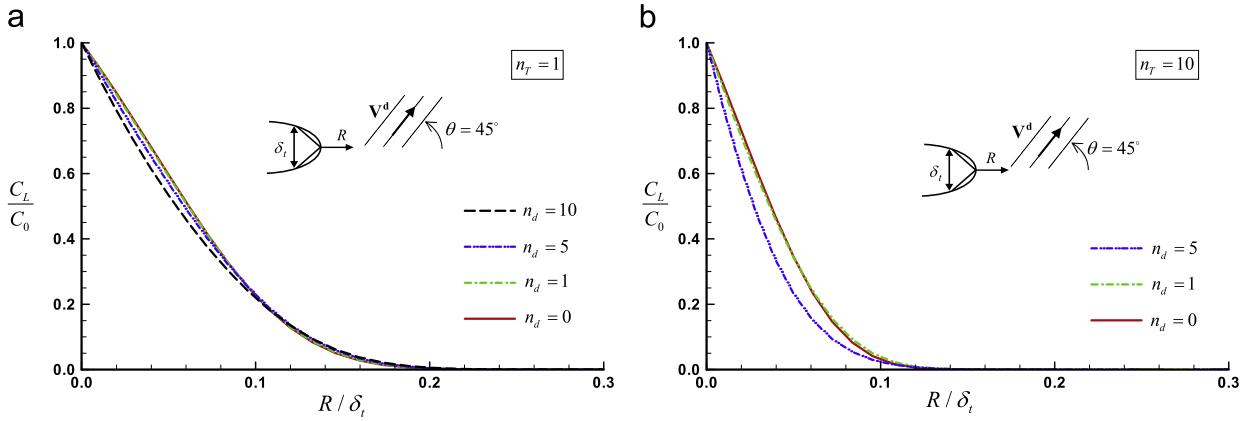

Fig. 6. Normalized NILS hydrogen concentration C_L/C_0 ahead of the crack tip for the *fcc* steel at $K_I = 100\ \text{MPa}\sqrt{\text{m}}$: (a) $n_T = 1$ and (b) $n_T = 10$. The crack opening displacement is $\delta_t = 40.99\ \mu\text{m}$ and $C_0 = 7.996 \times 10^{24}$ H atoms/m^3 (9.44×10^{-5} H atoms per solvent atom).

changing the dislocation velocity vector direction to 45° with respect to the crack plane, the hydrogen concentration ahead of the crack tip is similar for dislocation transport and lattice diffusion (Fig. 6). In fact, as for the bcc case shown in Fig. 3b, since hydrogen is transported by the dislocations away from the region ahead of the crack tip at a rate faster than it can diffuse through NILS, the NILS hydrogen concentration is found to be slightly lower than when dislocation transport is not considered in the analysis. With regard to the effect of dislocation transport on the trapped hydrogen populations, unlike the case for the bcc system there is a noticeable effect; compare Figs. 2 and 5. The reason is that dislocation traps are not saturated due to the low binding energy of hydrogen (10 kJ/mol compared to 50 kJ/mol in bcc), and as a result, the profiles of trapped hydrogen concentration vary along with those of the NILS hydrogen concentration (see also discussion in Section 4.1). In addition, the ratio θ_T/θ_L is not as large as in the bcc material and consequently, neither is the ratio $C_T/C_L = (\alpha N_T/\beta N_L)(\theta_T/\theta_L)$.

4. Parametric studies

In the following, the sensitivity of the dislocation transport model in relation to (i) the pressure of the gaseous hydrogen (magnitude of the boundary condition for the hydrogen concentration at the crack faces), (ii) the magnitude of the dislocation trap binding energy for the bcc system, (iii) the hydrogen diffusion coefficient, (iv) the loading rate, and (v) the mode of hydrogen uptake (internal vs. gaseous) is explored.

4.1. Hydrogen pressure (concentration boundary condition)

In Section 3, the prescribed NILS hydrogen concentration on the crack faces was in equilibrium with gaseous hydrogen at 1 atm (0.1 MPa). In this section, the effect of dislocation transport for a higher hydrogen gas pressure, i.e. 15 MPa, is considered.

For the bcc case, the new prescribed concentration on the crack face is $C_0' = 2.659 \times 10^{22}$ H atoms/m^3 ($=3.139 \times 10^{-7}$ H atoms per solvent atom) and as before, the specimen is loaded to $K_I = 100\ \mathrm{MPa}\sqrt{\mathrm{m}}$ at a stress intensity factor rate of $\dot{K}_I = 0.05\ \mathrm{MPa}\sqrt{\mathrm{m}}$/s. The results for the NILS hydrogen concentration at $K_I = 100\ \mathrm{MPa}\sqrt{\mathrm{m}}$ are shown in Fig. 7. Under the assumption that hydrogen does not change the dislocation density (i.e. $n_T = 1$), dislocation transport increases the peak NILS hydrogen concentration only by about 3% with $n_d = 10$, as shown in Fig. 7a. However, Fig. 7b shows that dislocation transport with an increased dislocation density, $n_T = 10$, increases the NILS hydrogen concentration at the peak location by about 30% when $n_d = 10$.

Certainly, this 30% increase is much smaller than the 520% increase calculated at the lower hydrogen pressure of 1 atm (Figs. 2 and 7). However, viewed in absolute terms, these increases have been brought about with respective hydrogen concentrations of $7.82 \times C_0 = 1.630 \times 10^{22}$ H atoms/m^3 and $0.69 \times C_0' = 1.841 \times 10^{22}$ H atoms/m^3, over and above that which could be delivered by lattice diffusion alone. The fact that these two amounts are almost the same relates to the high trap binding energy of hydrogen to dislocations in the bcc system, $W_B = 50$ kJ/mol, which dictates that the dislocations are almost saturated, $\theta_T \approx 1.0$, regardless of the hydrogen pressure on the crack faces. Hence the amount of hydrogen transported by mobile dislocations is almost independent of the hydrogen pressure. On the other hand, at higher pressures, it is expected that the dislocation densities and velocities will be higher than at lower pressures. This suggests that the effect of higher pressure in the present model should be treated with values of n_T and n_d that are greater than those at lower pressures. For instance, comparing the profiles $n_T = 10$, $n_d = 5$ (Fig. 2b, low pressure) and $n_T = 10$, $n_d = 10$ (Fig. 7b, high pressure), one sees

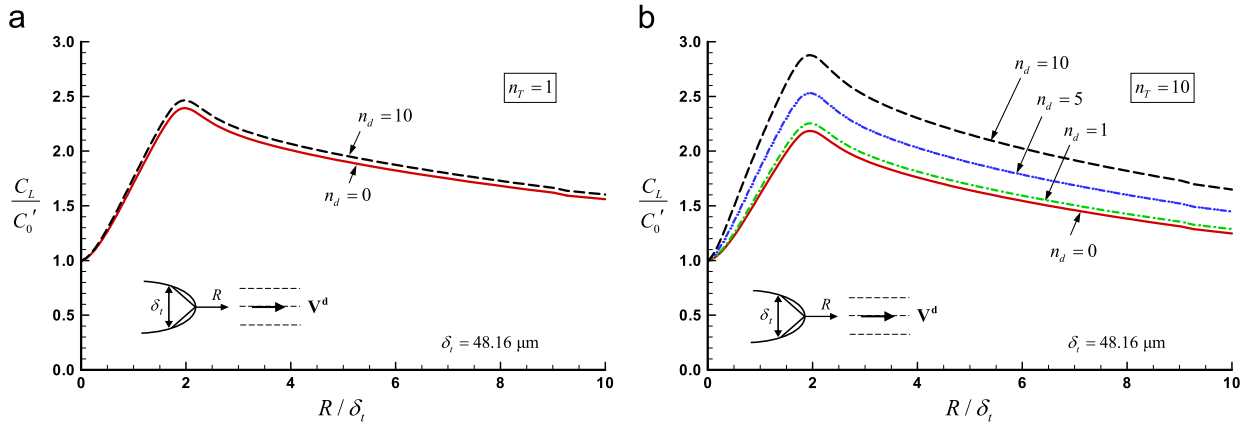

Fig. 7. Normalized hydrogen concentration in NILS C_L/C_0' ahead of the crack tip for the *bcc* steel at $K_I = 100\ \mathrm{MPa}\sqrt{\mathrm{m}}$ accounting for the effect of dislocation transport of hydrogen for different values of n_d with (a) $n_T = 1$ and (b) $n_T = 10$. The hydrogen concentration at the crack surface is $C_0' = 2.659 \times 10^{22}$ H atoms/m^3 (3.139×10^{-7} H atoms per solvent atom) which is in equilibrium with hydrogen gas pressure of 15 MPa.

that indeed the absolute increase of the lattice hydrogen concentration due to dislocation transport at low pressure is smaller than that at high pressure, i.e., $3.83 \times C_0 = 7.981 \times 10^{21}$ H atoms/m^3 vs. $0.69 \times C_0' = 1.841 \times 10^{22}$ H atoms/m^3.

For the fcc system, the new prescribed concentration on the crack face is $C_L = C_0' = 1.020 \times 10^{26}$ H atoms/m^3 ($=1.204 \times 10^{-3}$ H atoms per solvent atom) and as before, the specimen is loaded to $K_I = 100$ MPa$\sqrt{\text{m}}$ at stress intensity factor rate $\dot{K}_I = 0.01$ MPa$\sqrt{\text{m}}$/s. The results for the hydrogen profiles are almost the same as those at 1 atm hydrogen gas pressure shown in Fig. 5. This can be rationalized as follows: for the fcc case, the trap binding energy of hydrogen to dislocations is low ($W_B = 10$ kJ/mol) and therefore $\theta_T \ll 1.0$, given that also $\theta_L \ll 1.0$ for the pressures under consideration. Then, Eq. (1) yields $\theta_T/\theta_L \approx K_T$ which denotes that although the occupancies of NILS and trapping sites vary as the pressure increases from 1 atm to 15 MPa, their ratio remains constant. As a result,

$$\frac{\theta_T}{C_0} \approx K_T \frac{\theta_L}{C_0} = \frac{K_T}{\beta N_L}\frac{C_L}{C_0} = \frac{K_T}{\beta N_L}\phi \tag{15}$$

Substitution of θ_T/C_0 in the second and the last term of Eq. (13) gives

$$\frac{D}{D_{eff}}\frac{\partial \phi}{\partial \tau} + \frac{\alpha K_T}{\beta N_L}\frac{dN_T}{d\varepsilon^p}\frac{d\varepsilon^p}{d\tau}\phi - \frac{\partial^2 \phi}{\partial \xi_i \partial \xi_i} + \frac{\partial}{\partial \xi_i}\left(\phi \frac{\partial \psi}{\partial \xi_i}\right) + \frac{\partial}{\partial \xi_i}\left(\frac{\alpha K_T N_T^m}{\beta N_L}\phi \frac{V_i^d}{D/L}\right) = 0 \tag{16}$$

In the transport Eq. (16), the only term that depends on the reference concentration C_0 is the effective diffusion coefficient D_{eff} (see Eq. (11)). Due to the low binding energy of hydrogen to dislocations, the second term on the right hand side of Eq. (11) is much smaller than 1, so $D/D_{eff} \approx 1$. As a result, the non-dimensionalized hydrogen transport Eq. (16) is independent of the reference hydrogen concentration C_0 which can be taken to be the prescribed concentration on the crack faces. Therefore, the solution to the normalized hydrogen concentration field as furnished by Eq. (16) remains the same as the pressure changes. It is noted again that this feature of the solution to the transport problem is a consequence of the low binding energy of hydrogen to dislocations and the associated low occupancies of the lattice and trapping sites.

4.2. Dislocation trap binding energy for the bcc system

In this study, the crack faces are in equilibrium with gaseous hydrogen at 1 atm (0.1 MPa), as in Section 3.1 for the bcc system, but the dislocation trap binding energy, W_B, is reduced to either 30 or 40 kJ/mol. The normalized NILS and trapping hydrogen concentrations ahead of the crack tip at $K_I = 100$ MPa$\sqrt{\text{m}}$ are shown in Fig. 8. As the binding energy increases, so does θ_T (or C_T) and consequently the effect of dislocation transport on hydrogen accumulation (cf. Eq. (13)). For $n_T = 10$, $n_d = 10$, and hydrogen binding energies 30, 40, and 50 kJ/mol, the corresponding peak NILS hydrogen concentrations are larger by 2%, 113%, and 520% than those in the absence of dislocation transport ($n_d = 0$) (see, Figs. 8a, b, and 2b, respectively).

Looking at Fig. 8 ($W_B = 30$ or 40 kJ/mol), one sees that there is a local maximum in the trapped hydrogen concentration near the crack tip. Note that no such local maximum exists in Fig. 2 ($W_B = 50$ kJ/mol). In Fig. 2, the trap occupancy is unity and the trap density increases as the distance from the crack tip decreases toward a maximum as dictated by the model. Hence the concentration profile follows that of the trap density. On the other hand, in Fig. 8, trap occupancy changes with NILS occupancy. Hence, over a certain distance from the crack in which the trap density is constant, the trapped hydrogen concentration increases with distance from the crack tip. Beyond the point where the maximum is attained, the decrease of the trap density takes over and dictates the decrease in the trapped hydrogen concentration profile (Dadfarnia et al., 2008).

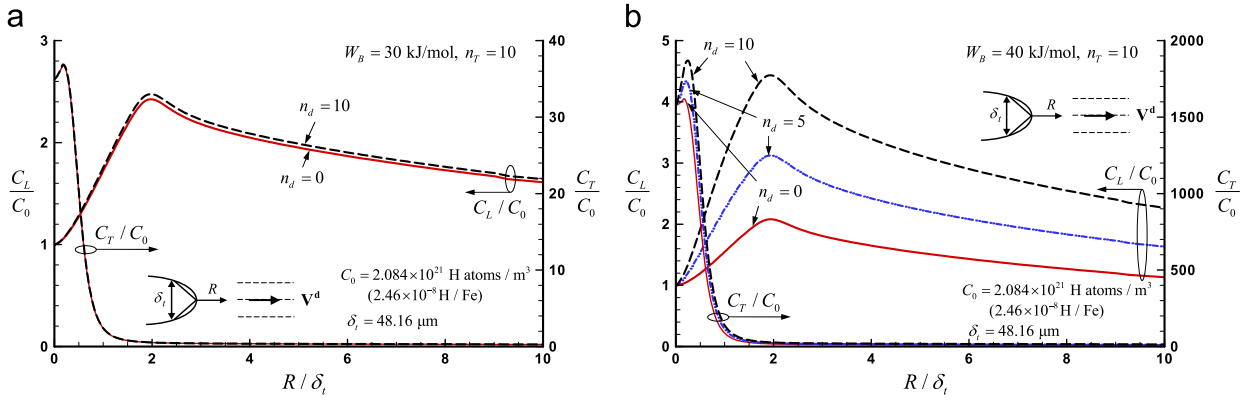

Fig. 8. Dependence of the normalized NILS and trapping hydrogen concentration ahead of the crack tip on the binding energy of hydrogen to dislocations in the bcc system; (a) $W_B = 30$ kJ/mol and (b) $W_B = 40$ kJ/mol. The stress intensity factor is $K_I = 100$ MPa$\sqrt{\text{m}}$ and the crack faces are exposed to hydrogen gas pressure of 1 atm.

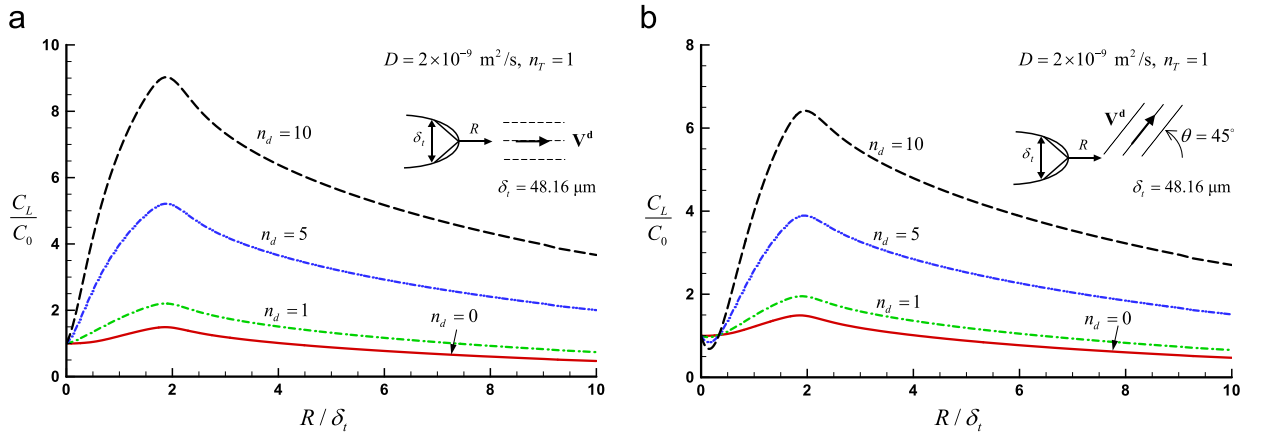

Fig. 9. Effect of hydrogen diffusion coefficient on hydrogen transport by dislocations in the bcc steel. Normalized hydrogen concentration in NILS C_L/C_0 ahead of the crack tip at $K_I = 100$ MPa$\sqrt{\text{m}}$ when the dislocation velocity $\mathbf{V^d}$ is (a) along the direction of the crack plane and (b) at an angle of 45° with the crack plane. The NILS hydrogen on the crack surface is $C_0 = 2.084 \times 10^{21}$ H atoms/m^3 (2.46×10^{-8} H atoms per solvent atom) which is the concentration in equilibrium with hydrogen gas pressure of 1 atm.

4.3. Hydrogen diffusion coefficient

To explore the effect of the hydrogen diffusion coefficient in the bcc steel, the hydrogen diffusion coefficient was decreased by an order of magnitude to $D = 2 \times 10^{-9}$ m^2/s; all other parameters were as reported in Table 1. Fig. 9 shows the NILS hydrogen concentration ahead of the crack tip at $K_I = 100$ MPa$\sqrt{\text{m}}$ under a hydrogen gas pressure of 1 atm. The difference between Fig. 9a and b is in the assumed direction of the dislocation velocity, $\mathbf{V^d}$. According to the last term of Eq. (13), the influence of dislocation transport on the NILS hydrogen concentration development is proportional to the inverse of the diffusion coefficient D. Comparing Fig. 9a ($D = 2 \times 10^{-9}$ m^2/s) and Fig. 2a ($D = 2 \times 10^{-8}$ m^2/s) for the cases when $n_d = 10$ and $n_T = 1$, it can be seen that decreasing the hydrogen diffusion coefficient causes a greater increase in the NILS hydrogen concentration peak compared to that in the absence of dislocation transport. The increase is 6.1 and 1.4 for $D = 2 \times 10^{-9}$ m^2/s and $D = 2 \times 10^{-8}$ m^2/s, respectively. Changing the direction of the dislocation vector to 45° does not change the fact that with a lower diffusion coefficient dislocation transport results in a greater increase of the concentration relative to the absence of dislocation transport; compare Figs. 9b and 3a. The increase is 4.3 times compared to 1.3 for the faster diffusion coefficient. In summary, the effect of dislocation transport on increasing the NILS hydrogen concentrations is larger when the diffusion through NILS is slower. This contrast is even more marked for $n_T = 10$. Results for the fcc system follow the same trend as for the bcc system (Fig. 10).

4.4. Effect of loading rate

For the HELP mechanism to continue to operate, the dislocation velocity must not exceed some critical value, which can

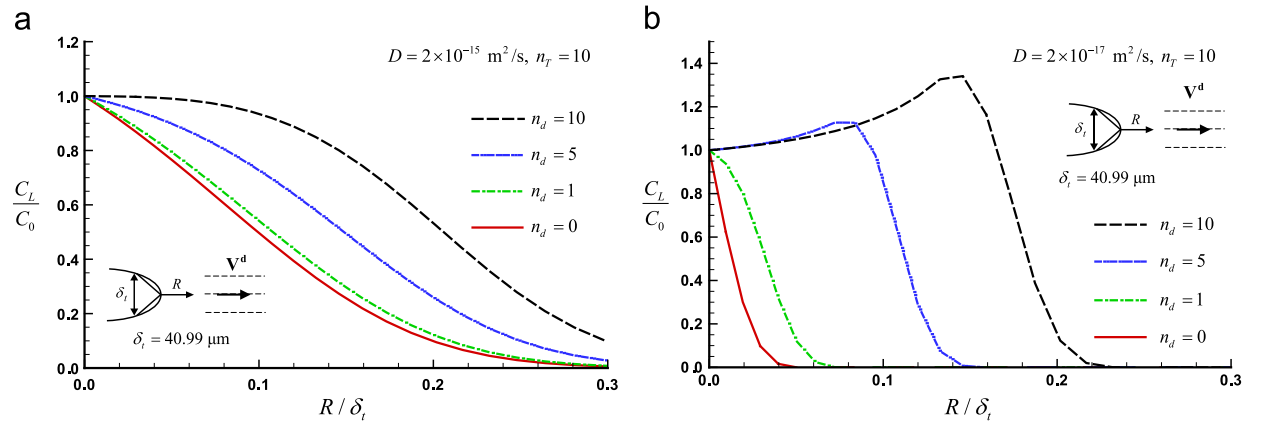

Fig. 10. Effect of hydrogen diffusion coefficient on dislocation transport of hydrogen for the *fcc* steel. Normalized NILS hydrogen concentration C_L/C_0 ahead of the crack tip at $K_I = 100$ MPa$\sqrt{\text{m}}$ when the hydrogen diffusion coefficient is (a) $D = 2 \times 10^{-15}$ m^2/s and (b) $D = 2 \times 10^{-17}$ m^2/s. The NILS hydrogen on the crack surface is $C_0 = 7.996 \times 10^{24}$ H atoms/m^3 (9.44×10^{-5} H atoms per solvent atom) which is the concentration in equilibrium with hydrogen gas pressure of 1 atm.

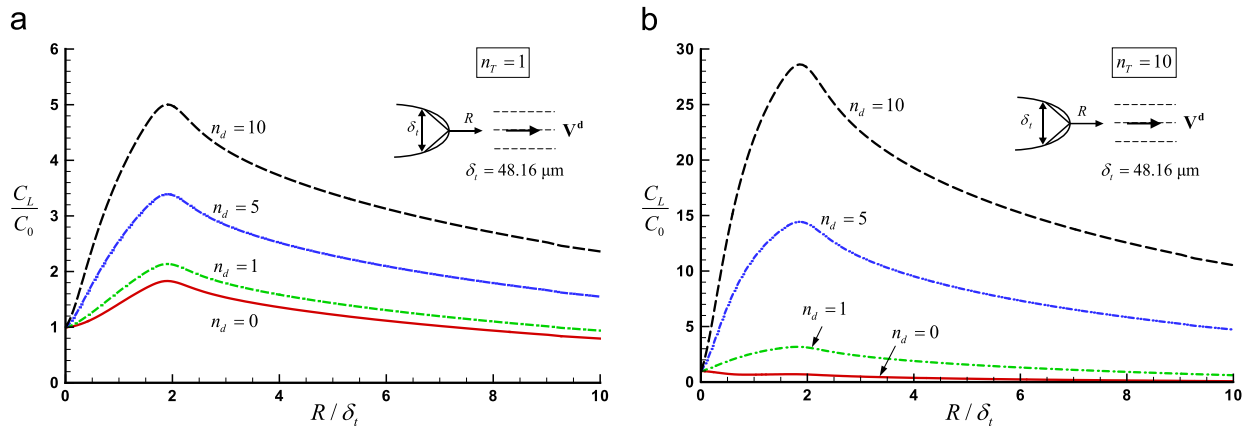

Fig. 11. Normalized hydrogen concentration C_L/C_0 in NILS ahead of the crack tip for the bcc steel at $K_I = 100$ MPa$\sqrt{\text{m}}$, loading rate $\dot{K}_I = 0.2$ MPa$\sqrt{\text{m}}$/s, and (a) $n_T = 1$ and (b) $n_T = 10$. The hydrogen concentration at the crack faces is $C_0 = 2.084 \times 10^{21}$ H atoms/m^3 (2.46×10^{-8} H atoms per solvent atom). The direction of the dislocation velocity vector $\mathbf{V^d}$ with respect to the crack plane is shown on the figure.

be calculated approximately from the following (Tien et al., 1975, 1976):

$$v_c = \frac{D}{RT}\frac{W_B}{30b}. \tag{17}$$

This yields for the bcc and fcc metals, critical velocities of $v_c^{bcc} \approx 53$ m/s and $v_c^{fcc} \approx 10^{-7}$ m/s, respectively. These values set the maximum values of the loading rate that should be considered. Loading rates of $\dot{K}_I = 0.2$ MPa$\sqrt{\text{m}}$/s and $\dot{K}_I = 0.01$ MPa$\sqrt{\text{m}}$/s respectively for the bcc and fcc metals were considered. The resultant dislocation velocities remain below the critical breakaway velocities.[1]

The bcc steel was loaded to $K_I = 100$ MPa$\sqrt{\text{m}}$ at an intensity factor rate $\dot{K}_I = 0.2$ MPa$\sqrt{\text{m}}$/s which is higher than the rate $\dot{K}_I = 0.05$ MPa$\sqrt{\text{m}}$/s used in the simulations reported in Section 3.1. The profiles of hydrogen concentration at NILS ahead of the crack tip at the end of loading are shown in Fig. 11 as a function of normalized distance R/δ_t from the crack tip. From Figs. 2 and 11, it is seen that the hydrogen concentration profiles are clearly higher for the higher loading rate although the loading time is correspondingly shorter (500 s as opposed to 2000 s for $\dot{K}_I = 0.05$ MPa$\sqrt{\text{m}}$/s). Higher loading rates yield higher plastic strain rates which are associated with larger fluxes of mobile dislocations and hence larger amounts of hydrogen transported by them. The effect is discussed further in Section 5.

4.5. Internal hydrogen

Thus far, the development of hydrogen concentration profiles of initially non-charged specimens were explored for the case in which the crack faces were exposed to gaseous hydrogen upon loading. In this section, the influence of internal hydrogen is considered.

The bcc case was considered for an initial hydrogen concentration of $C_L(t=0) = C_0 = 2.084 \times 10^{21}$ H atoms/m^3 ($=2.46 \times 10^{-8}$ H atoms per solvent atom) throughout. As before, the specimen was loaded at a stress intensity factor rate of $\dot{K}_I = 0.05$ MPa$\sqrt{\text{m}}$/s from the stress-free state to $K_I = 100$ MPa$\sqrt{\text{m}}$. It was assumed that the crack and outer boundary of the domain are impermeable to hydrogen, that is, zero flux boundary condition was prescribed.

The NILS hydrogen profiles along the axis of symmetry ahead of the crack tip for various values of n_T and n_d are presented in Fig. 12. For the case of no hydrogen effect on dislocation density, i.e. $n_T = 1$, Fig. 12a shows that, when $n_d = 10$, the NILS hydrogen concentration at the peak location is higher by 12% relative to the case of no dislocation transport ($n_d = 0$). Also, dislocations, by carrying hydrogen away from the crack tip, may deplete the lattice over a substantial fraction of the fracture process zone. This depletion is more pronounced, the larger the effect of hydrogen on the dislocation density, $n_T > 1$. Increased dislocation density results in increased demand for hydrogen by the traps. For the closed system under consideration, there is no supply of hydrogen though the crack surfaces and hence the lattice gets locally depleted. This is evident from Fig. 12b by considering the baseline result of no dislocation transport, $n_d = 0$.

Lattice depletion is also the case for the insulated fcc system. Fig. 13 shows the NILS hydrogen profiles along the axis of symmetry ahead of the crack tip for the fcc case and the local depletion due to the generation of traps and hydrogen carried

[1] For the fcc steel specimen loaded at a stress intensity factor rate $\dot{K}_I = 0.01$ MPa$\sqrt{\text{m}}$/s, the maximum crack tip strain rate was calculated to be about $\dot{\varepsilon}^p \approx 2 \times 10^{-4}$/s. The maximum dislocation density in the neighborhood of the crack tip for $\varepsilon^p > 0.5$ is about 10^{16} line length/m^3. In a worst case scenario with a mobile dislocation density only about 1% of the total dislocation density, the maximum dislocation velocity is calculated from Eq. (14) to be about 8×10^{-9} m/s which is an order of magnitude smaller than the breakaway velocity. Therefore, even if we assume that hydrogen increases the dislocation velocity by a factor of 10 ($n_d = 10$) the velocity of dislocations is still below the critical breakaway velocity. However, faster loading rates can change this situation.

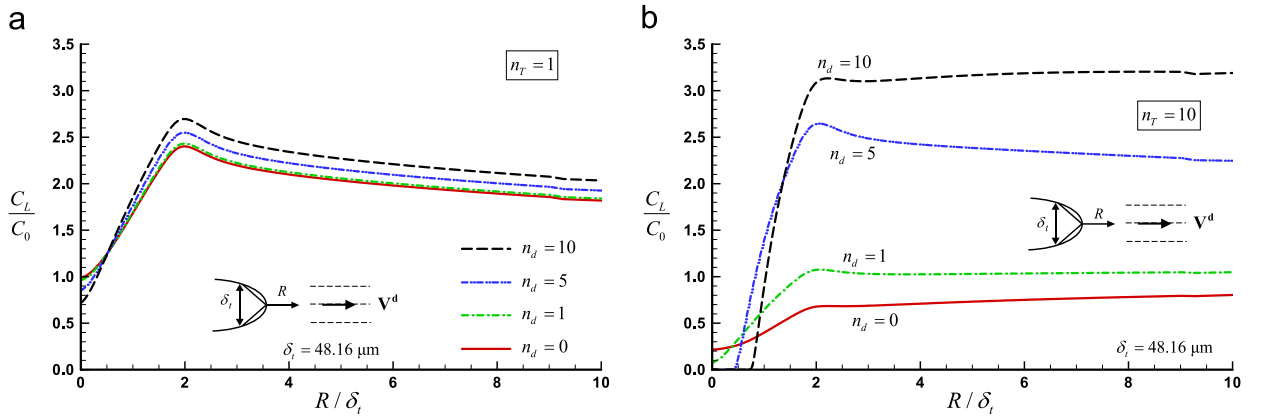

Fig. 12. Normalized NILS hydrogen concentration C_L/C_0 ahead of the crack tip for the *bcc* steel at $K_I = 100$ MPa$\sqrt{\text{m}}$ when all domain boundaries (Fig. 1) are impermeable to hydrogen (zero flux boundary condition) with (a) $n_T = 1$ and (b) $n_T = 10$. The parameter $C_0 = 2.084 \times 10^{21}$ H atoms/m^3 (2.46×10^{-8} H atoms per solvent atom) is the initial NILS hydrogen concentration.

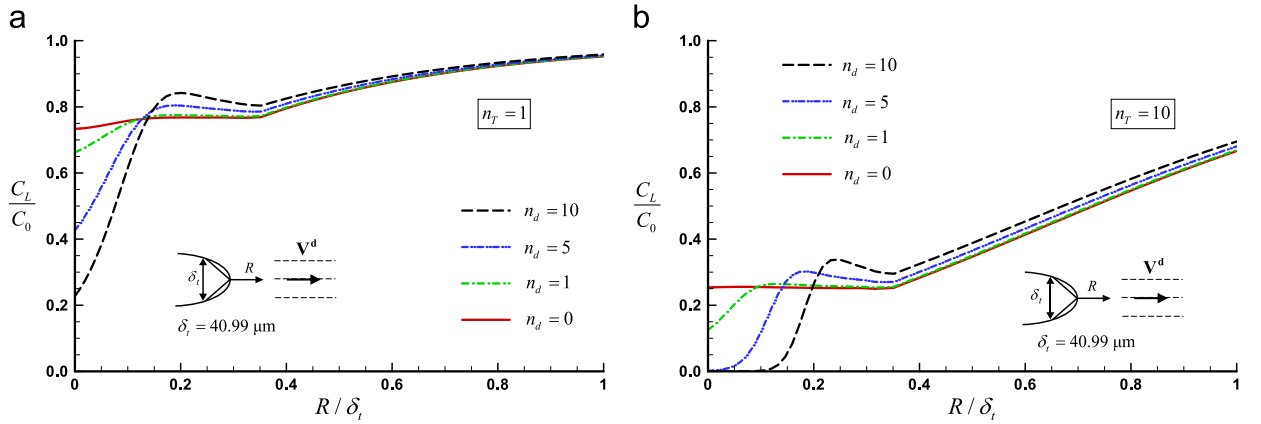

Fig. 13. Normalized NILS hydrogen concentration C_L/C_0 ahead of the crack tip for the *fcc* steel at $K_I = 100$ MPa$\sqrt{\text{m}}$ when all domain boundaries (Fig. 1) are impermeable to hydrogen (zero flux boundary condition) with (a) $n_T = 1$ and (b) $n_T = 10$. The initial NILS hydrogen concentration is $C_0 = 7.996 \times 10^{24}$ H atoms/m^3 (9.44×10^{-5} H atoms per solvent atom).

away by dislocations. Unlike the bcc system, in which dislocation transport increases the hydrogen concentration over a distance several times the crack tip opening displacement ($R > \delta_t$), in the fcc system, hydrogen transport by dislocations influences the hydrogen concentration only in the region very close to the crack tip (i.e. $R < 0.4\delta_t$). This difference is due to the fact that the trapping models and lattice concentration levels in bcc and fcc systems differ. For the model of trap density used for fcc in this work, trap density reduces at a faster rate following the reduction of the plastic strain with distance from the crack tip. Moreover, the lattice concentration in the fcc system is much larger than in the bcc system. Hence, the effect of dislocation transport on the NILS concentration in the fcc system is less than that in the bcc system for the models explored.

It should be noted that the depletion of the lattice hydrogen concentration may affect the profile of hydrogen concentration at trapping sites. For the bcc system with $n_T = 1$, Fig. 12a, the trapped hydrogen concentrations are similar to the ones shown in Fig. 2a with their maximum at the crack tip. Due to the high binding energy, the traps are saturated and the difference in lattice concentration does not affect the profile of hydrogen concentration at trapping sites. However, for $n_T = 10$, Fig. 12b, the lattice is completely depleted at the crack tip when the effect of hydrogen on dislocation velocity is considered with $n_d = 5$ or 10. In that case, hydrogen trapped at dislocation is also depleted due to equilibrium between lattice and trapped hydrogen concentration, Eq. (1). For the fcc system, the trapped hydrogen concentration profile follows the NILS profile due to the low binding energy of hydrogen in the fcc system as discussed in Section 3.2.

5. Conclusions

A model was presented for hydrogen transport in an elastoplastically deforming material accounting for dislocation transport, stress driven diffusion through interstitial lattice sites, and trapping at mobile and immobile dislocations. The impact of this additional transport mechanism was explored for a cracked specimen exposed to a gaseous hydrogen

atmosphere or internal hydrogen under small scale yielding conditions. Specifically, dislocation transport was investigated by considering hydrogen-induced increases of the dislocation velocity or density by as much as 10 times relative to the hydrogen free material. In the simulations, the material parameters were chosen for a bcc X70/X80 type pipeline steel (large hydrogen diffusivity) and a forged Nitronic 40 stainless steel (low hydrogen diffusivity). The primary findings can be summarized as follows:

The effect of dislocation transport on the hydrogen population developments in NILS is governed by the dimensionless group $\theta_T \dot{\varepsilon}^p L/DC_0$, where θ_T is the occupancy of dislocation trapping sites, $\dot{\varepsilon}^p$ is the plastic strain rate, L is a geometric dimension, D is the hydrogen diffusion coefficient, and C_0 is a reference concentration. Thus, dislocation transport has a larger effect on hydrogen accumulation in front of the crack tip in materials with a lower lattice diffusion coefficient for hydrogen. In addition, for obvious reasons, the effect becomes larger when the binding energy of hydrogen to dislocations is larger.

For gaseous charging through the crack tip, dislocation transport can deliver hydrogen to the fracture process zone at concentrations much higher than those delivered by lattice diffusion alone. For the bcc systems, lattice diffusion alone delivers to the peak location ahead of a crack tip hydrogen concentrations about 3 times as large as the nominal concentration whereas dislocation transport can help deliver about 9 times as the nominal for binding energy 50 kJ/mol. In addition, dislocation transport can deliver hydrogen at distances further afield at larger concentrations than lattice diffusion alone. These results are qualitatively in line with the proposition by Martin et al. (2011a, 2011b, 2012a), Nagao et al. (2012) and most recently Wang et al. (2014) that the lattice ahead of the crack tip, even at distances larger than $3\delta_t$, i.e. the typical size of the fracture process zone, experiences severe plastic straining accentuated by the presence of hydrogen.

For gaseous charging through the crack tip, dislocation transport in bcc steels results in normalized hydrogen concentrations that depend on pressure when the dislocation traps are saturated. Pressure independence of the normalized concentration holds for fcc steels due to the fact that the ratio of trap occupancy to lattice occupancy is constant and equal to the equilibrium constant.

For gaseous charging through the crack tip, increasing the loading rate results in larger dislocation fluxes and hence in higher hydrogen accumulation ahead of the crack tip if the increase in loading rate does not cause the dislocations to break away from their atmospheres. On the other hand, for internal hydrogen, dislocation transport tends to deplete the crack tip region.

The implication of these calculations on the experimental results of Sofronis, Robertson and coworkers are now considered (Martin et al., 2011a, 2011b, 2012a; Nagao et al., 2012; Wang et al., 2014). The increase of hydrogen transport with increasing dislocation density may allow for a feedback mechanism whereby hydrogen transport allows for areas with increasing dislocation activity due to hydrogen-enhanced plasticity, and the resulting increased dislocation density leads to increased hydrogen transport effects. These high hydrogen concentrations, higher than predicted by other models, could create regions where different mechanisms operate, negating criticisms that it is impossible to achieve high hydrogen concentrations. The effect of dislocation direction also suggests that different grain orientations may be affected differently. As such, local conditions, defined by the local microstructural features, such as dislocation structures, grain boundaries, and variations between grains, and the resulting hydrogen concentration due to the evolving microstructure and the attendant local stresses, could vary significantly. As a result, different mechanisms could be active over different areas, resulting in variations in fracture morphology, consistent with experimental observation.

Lastly, the calculations indicate that the hydrogen populations ahead of a crack tip in the bcc system are larger with increasing strain rate. This is counterintuitive given that the embrittlement susceptibility decreases with increasing strain rate (Hirth, 1980). Here it should be remembered that the present results are based on the equilibrium assumption between hydrogen in the lattice and hydrogen trapped in the dislocations. With increasing strain rate, there may not be enough time for this equilibrium to be established and hence moving dislocations carry less hydrogen, as Hashimoto and Latanision (1988) point out. Hence the present equilibrium model should be modified to account for this lack of dynamic equilibrium between the lattice and trapped hydrogen if to be applied at high strain rates.

Acknowledgments

The authors gratefully acknowledge the support of the International Institute for Carbon Neutral Energy Research (WPI-I2CNER), sponsored by the World Premier International Research Center Initiative (WPI), MEXT, Japan. M.D. and P.S. also acknowledge discussions with Professor C. Pantano-Rubino on the numerical simulations. I. M. R. acknowledges support from the National Science Foundation through Award No. CMMI-1406462.

References

Bastien, P., Azou, P., 1951. Effect of hydrogen on the deformation and fracture of iron and steel in simple tension, In: Proceedings of the First World Metallurgical Congress, Baldwin W.M. (Ed.), ASM, Cleveland, OH, pp. 535–552.

Clark, W.A.T., Wagoner, R.H., Shen, Z.Y., Lee, T.C., Robertson, I.M., Birnbaum, H.K., 1992. On the criteria for slip transmission across interfaces in polycrystals. Scr. Metall. Mater. 26 (2), 203–206.

Dadfarnia, M., Somerday, B.P., Sofronis, P., Robertson, I.M., Stalheim, D., 2009. Interaction of hydrogen transport and material elastoplasticity in pipeline steels. J. Press. Vess. Technol. 131 (4). 041404-1–041404-13.

Dadfarnia, M., Sofronis, P., Neeraj, T., 2011. Hydrogen interaction with multiple traps: can it be used to mitigate embrittlement? Int. J. Hydrog. Energy 36 (16), 10141–10148.
Dadfarnia, M., Sofronis, P., Somerday, B.P., Robertson, I.M., 2008. On the small scale character of the stress and hydrogen concentration fields at the tip of an axial crack in steel pipeline: effect of hydrogen-induced softening on void growth. Int. J. Mater. Res. 99 (5), 557–570.
Frankel, G.S., Latanision, R.M., 1986. Hydrogen transport during deformation in nickel: Part II. single crystal nickel. Metall. Trans. A 17 (5), 869–875.
Ferreira, P.J., Robertson, I.M., Birnbaum, H.K., 1998. Hydrogen effects on the interaction between dislocations. Acta Mater. 46 (5), 1749–1757.
Gerberich, W.W., Marsh, P.G., Hoehn, J.W., 1996. Hydrogen induced cracking mechanisms – are there critical experiments?. In: Thompson, A.W., Moody, N. R. (Eds.), Hydrogen Effects in Materials. TMS, Warrendale, PA, pp. 539–551.
Gilman, J.J., 1969. In: Micromechanics of Flow in SolidsMcGraw-Hill, New York.
Hwang, C., Bernstein, I.M., 1986. Dislocation transport of hydrogen in iron single crystals. Acta Metall. 34 (6), 1001–1010.
Hirth, J.P., Johnson, H.H., 1983. On the transport of hydrogen by dislocations. In: Latanision, R.M., Pickens, J.R. (Eds.), Proceedings of a NATO Advanced Research Institute on Atomistics of Fracture. Plenum Press, New York, pp. 771–787.
Hirth, J.P., Carnahan, B., 1978. Hydrogen adsorption at dislocations and cracks in Fe. Acta Metall. 26 (12), 1795–1803.
Hirth, J.P., 1980. Effects of hydrogen on the properties of iron and steel. Metall. Trans. A 11 (6), 861–890.
Hashimoto, M., Latanision, R.M., 1988. Experimental study of hydrogen transport during plastic deformation in iron. Metall. Trans. A 19 (11), 2789–2798.
Itoh, G., Jinkoji, T., Kanno, M., Koyama, K., 1997. Effect of impurity hydrogen on the deformation and fracture in an Al-5 mass Pct mg alloy. Metall. Mater. Trans. A 28 (11), 2291–2295.
Irwin, G.R., 1960. Fracture mechanics. In: Goodier, J.N., Hoff, N.J. (Eds.), Proceedings of the 1st Symposium of Naval Structural Mechanics on Structural Mechanic. Pergamon Press, New York, pp. 557–594.
Kurkela, M., Latanision, R.M., 1979. The effect of plastic deformation on the transport of hydrogen in nickel. Scr. Metall. 13 (10), 927–932.
Kumnick, A.J., Johnson, H.H., 1980. Deep trapping states for hydrogen in deformed iron. Acta Metall. 28 (1), 33–39.
Lassila, D.H., Birnbaum, H.K., 1986. The effect of diffusive hydrogen segregation on fracture of polycrystalline nickel. Acta Metall. 34 (7), 1237–1243.
Lassila, D.H., Birnbaum, H.K., 1987. Intergranular fracture of nickel: the effect of hydrogen–sulphur co-segregation. Acta Metall. 35 (7), 1815–1822.
Lassila, D.H., Birnbaum, H.K., 1988. The effect of diffusive segregation on the fracture of hydrogen charged nickel. Acta Metall. 36 (10), 2821–2825.
Ladna, B., Birnbaum, H.K., 1987. SIMS study of hydrogen at the surface and grain boundaries of nickel bicrystals. Acta Metall. 35 (10), 2537–2542.
Lee, T.C., Robertson, I.M., Birnbaum, H.K., 1990a. In situ transmission electron microscope deformation study of the slip transfer mechanisms in metals. Metall. Trans. A 21 (9), 2437–2447.
Lee, T.C., Robertson, I.M., Birnbaum, H.K., 1990b. TEM in situ deformation study of the interaction of lattice dislocations with grain boundaries in metals. Philos. Mag. A 62 (1), 131–153.
Liang, Y., Sofronis, P., 2003. Micromechanics and numerical modeling of the hydrogen-particle–matrix interactions in nickel-base alloys. Model. Simul. Mater. Sci. Eng. 11 (4), 523–551.
Liang, Y., Sofronis, P., Dodds Jr., R.H., 2004. Interaction of hydrogen with crack-tip plasticity: effects of constraint on void growth. Mater. Sci. Eng. A 366 (2), 397–411.
Liang, Y., Ahn, D.C., Sofronis, P., Dodds Jr., R.H., Bammann, D., 2008. Effect of hydrogen trapping on void growth and coalescence in metals and alloys. Mech. Mater. 40 (3), 115–132.
Martin, M.L., Fenske, J.A., Liu, G.S., Sofronis, P., Robertson, I.M., 2011a. On the formation and nature of quasi-cleavage fracture surfaces in hydrogen embrittled steels. Acta Mater. 59 (4), 1601–1606.
Martin, M.L., Robertson, I.M., Sofronis, P., 2011b. Interpreting hydrogen-induced fracture surfaces in terms of deformation processes: a new approach. Acta Mater. 59 (9), 3680–3687.
Martin, M.L., Somerday, B.P., Ritchie, R.O., Sofronis, P., Robertson, I.M., 2012a. Hydrogen-induced intergranular failure in nickel revisited. Acta Mater. 60 (6–7), 2739–2745.
Martin, M.L., Sofronis, P., Robertson, I.M., Awane, T., Murakami, Y., 2013. A microstructural based understanding of hydrogen-enhanced fatigue of stainless steels. Int. J. Fatigue 57, 28–36.
Martin, M.L., Auger, T., Johnson, D.D., Robertson, I.M., 2012b. Liquid–metal-induced fracture mode of martensitic T91 steels. J. Nucl. Mater. 426 (1–3), 71–77.
Martin, M.L., Nagao, A., Robertson, I.M., Sofronis, P., 2014. Hydrogen-enhanced plasticity and failure revisited. In: Somerday, B.P., Sofronis, P. (Eds.), 2012 International Hydrogen Conference: Hydrogen–Materials Interactions. ASME Press, New York, NY, pp. 489–496.
McLellan, R.B., 1979. Thermodynamics and diffusion behavior of interstitial solute atoms in non-perfect solvent crystals. Acta Metall. 27 (10), 1655–1663.
Moody, N.R., Robinson, S.L., Garrison, W.M.J., 1990. Hydrogen effects on the properties and fracture modes of iron-based alloys. Res Mech. 30 (2), 143–206.
Nagao, A., Smith, C.D., Dadfarnia, M., Sofronis, P., Robertson, I.M., 2012. The role of hydrogen in hydrogen embrittlement fracture of lath martensitic steel. Acta Mater. 60 (13–14), 5182–5189.
Nagao, A., Kuramoto, S., Kanno, M., 1998. Hydrogen microprint technique applied to observe impurity hydrogen in aluminum during deformation. In: Proceedings of the 1998 TMS Annual Meeting. Mishra B., (Ed.). TMS, Warrendale, PA, pp. 867–875.
Novak, P., Yuan, R., Somerday, B.P., Sofronis, P., Ritchie, R.O., 2010. A statistical, physical-based, micro-mechanical model of hydrogen-induced intergranular fracture in steel. J. Mech. Phys. Solids 58 (2), 206–226.
Oriani, R.A., 1970. The diffusion and trapping of hydrogen in steel. Acta Metall. 18 (1), 147–157.
Robertson, I.M., 2001. The effect of hydrogen on dislocation dynamics. Eng. Fract. Mech. 68 (6), 671–692.
Sofronis, P., Birnbaum, H.K., 1995. Mechanics of the hydrogen-dislocation–impurity interactions – I. Increasing shear modulus. J. Mech. Phys. Solids 43 (1), 49.
Sofronis, P., McMeeking, R.M., 1989. Numerical analysis of hydrogen transport near a blunting crack tip. J. Mech. Phys. Solids 37 (3), 317–350.
Staykov, A., Yamabe, J., Somerday, B.P., 2014. Effect of hydrogen gas impurities on the hydrogen dissociation on iron surface. Int. J. Quantum Chem. 114 (10), 626–635.
San Marchi, C., Somerday, B.P., Robinson, S.L., 2007. Permeability, solubility and diffusivity of hydrogen isotopes in stainless steels at high gas pressures. Int. J. Hydrog. Energy 32 (1), 100–116.
Tien, J.K., Richards, R.J., Buck, O., Marcus, H.L., 1975. Model of dislocation sweep-in of hydrogen during fatigue crack growth. Scr. Metall. 9 (10), 1097–1101.
Tien, J.K., Thompson, A.W., Bernstein, I.M., Richards, R.J., 1976. Hydrogen transport by dislocations. Metall. Trans. A 7 (6), 821–829.
Tien, J.K., 1976. Diffusion and the dislocation sweeping mechanism for hydrogen transport. In: Bernstein, I.M., Thompson, A.W. (Eds.), Effects of Hydrogen on Behavior of Materials. TMS-AIME, New York, NY, pp. 309–326.
Taha, A., Sofronis, P., 2001. A micromechanics approach to the study of hydrogen transport and embrittlement. Eng. Fract. Mech. 68 (6), 803–837.
Thomas, G.J., 1981. Hydrogen trapping in FCC metals. In: Proceedings of the 3rd International Conference on Effect of Hydrogen on Behavior of Materials. Hydrogen Effects in Metals. Bernstein I.M., Thompson A.W. (Eds.). The Metallurgical Society of AIME, Warrendale, PA, pp. 77–85.
Wang, S., Martin, M.L., Sofronis, P., Ohnuki, S., Hashimoto, N., Robertson, I.M., 2014. Hydrogen-induced intergranular failure of iron. Acta Mater. 69, 275–282.
Windle, A.H., Smith, G.C., 1968. Effect of hydrogen on plastic deformation of nickel single crystals. Met. Sci. J. 2, 187–191.